A True Time Delay Beamforming System Incorporating a Wavelength Tunable Optical Phase-Lock Loop

Howard R. Rideout, Joe S. Seregelyi, and Jianping Yao, *Senior Member, IEEE*

***Abstract*—A true time delay (TTD) beamforming system incorporating a wavelength tunable optical phase-lock loop (OPLL) module is proposed and experimentally demonstrated. In the proposed system, instead of using a high-frequency intensity modulator to modulate the optical carrier with an RF signal, we use two laser diodes (LDs) that are phase locked to generate an RF signal, which is then sent to a fiber Bragg grating (FBG) prism to produce different time delays. Since no optical intensity modulator is used, the system can operate at much higher frequencies with a reduced cost. In addition, the use of only two wavelengths eliminates the power-penalty problem caused by chromatic dispersion. In the proposed approach, the wavelengths from the two LDs are phase-locked using a frequency-discriminator-aided OPLL. A TTD beamforming system, using the OPLL in combination with an FBG prism to achieve tunable time delays, is investigated. Experimental time-delay results are provided.**

***Index Terms*—Beamforming, external cavity laser (ECL), fiber Bragg grating (FBG), microwave photonics, optical delay line, optical heterodyne, optical phase-lock loop (OPLL), phased-array antenna (PAA), true time delay (TTD).**

I. Introduction

PHOTONIC true time delay (TTD) beamforming is considered a promising technique for wideband phased-array antenna (PAA) systems and has been extensively investigated in the last decade [1]–[7]. Compared to conventional antennas, PAAs have many advantages, such as high directivity, low visibility, beam pointing agility, and dynamic beam patterning, which make them attractive for applications such as high-performance radar and broadband wireless access systems [7], [8]. PAAs are usually implemented using electrical phase shifters. However, the use of phase shifters suffers from the well-known beam-squint problem, which leads to the corruption of the radiation beam for broadband operation [9]. This problem can be avoided by using a linear, rather than a fixed, phase shift [3], [10]. One efficient way to achieve a linear phase shift is to use TTD. The TTD can be obtained in the electrical domain, for example, using coplanar microstrip delay lines, at the cost of narrow bandwidth, heavy weight, and large size [11]. An alternative way to implement TTD is to use optical delay lines. Many approaches used in generating tunable optical delay lines have been proposed in the last few years [12]–[21]. The advantages offered by this technique include low loss, small size, large bandwidth, and immunity to electromagnetic interference [4], [5].

The method implemented here, to generate the required electrical phase shift for PAA beamforming, uses uniform fiber Bragg grating (FBG) delay lines [6]. By tuning the system wavelength to different values, the reflection position along the grating delay line is changed, varying the time delay of the optical signal, and thus, the phase of the recovered electrical signal at each array element. This arrangement will be discussed in further detail in Section II.

A TTD beamforming system can be fed by an optical signal in a variety of ways, depending on the architecture. FBG-based approaches are usually fed by a single wavelength optical source that is externally modulated by an RF signal [6]. For some applications, TTD beamforming systems have to operate at higher frequencies, which require expensive high-speed external modulators. In addition, conventional intensity modulation generates a signal with two sidebands plus a carrier, which suffers from chromatic dispersion leading to a power penalty. To solve these problems, the use of a coherent optical source based on the heterodyning of two lasers has been suggested [22]–[24]. In this paper, we propose and demonstrate the use of a frequency discriminator-aided optical phase-lock loop (OPLL) as the coherent optical source, in combination with a uniform FBG-delay line TTD beamforming module to achieve tunable time delays.

II. System Description

A. Optical Phase-Locked Loop (OPLL)

Optical heterodyning is the beating of two wavelengths at a photodetector (PD) to produce a microwave signal with a frequency corresponding to the offset between the two optical wavelengths. This technique offers the advantages of very high frequency generation (limited only by the bandwidth of the PD), large tunable range [25], high output power, and minimization of the chromatic-dispersion-induced power penalty [26].

This last benefit comes from the single sideband (SSB) nature of the OPLL source. This advantage of SSB versus

Manuscript received September 2, 2006; revised February 20, 2007. This work was supported in part by the Natural Sciences and Engineering Research Council (NSERC) of Canada.

H. R. Rideout and J. S. Seregelyi are with the Communications Research Centre Canada, Ottawa, ON K2H 8S2, Canada.

J. Yao is with the Microwave Photonics Research Laboratory, School of Information Technology and Engineering, University of Ottawa, Ottawa, ON K1N 6N5, Canada (e-mail: jpyao@site.uOttawa.ca).

Digital Object Identifier 10.1109/JLT.2007.899189

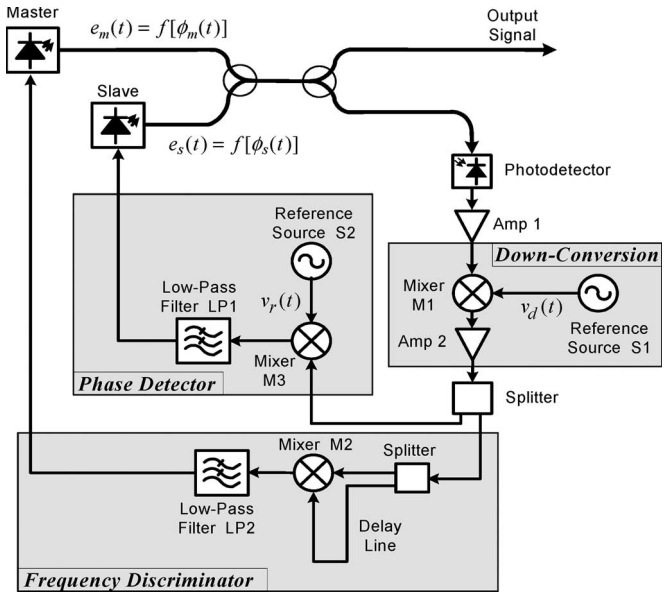

Fig. 1. Frequency-discriminator-aided OPLL.

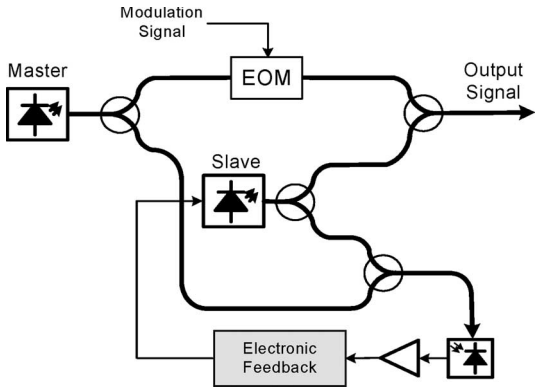

Fig. 2. Configuration of an OPLL for data modulation of one wavelength.

double sideband modulation (DSB) in avoiding a significant power penalty has been documented in [27] and [28].

For two free-running laser sources, the individual phase noise of each laser source contributes directly to the phase noise in the generated microwave signal. To generate a microwave signal with low phase noise, the two optical wavelengths must be phase-correlated. One method to achieve this is to use an OPLL.

An OPLL is a dual wavelength source with a wavelength spacing corresponding to the desired microwave output frequency [29], [41]. The two optical wavelengths are phase-locked through a feedback loop, and by beating the two wavelengths at a PD, a microwave carrier signal with low phase noise is generated. Fig. 1 shows a schematic of the discriminator-aided OPLL circuit. A discussion on this design is presented in [30], with modifications presented in [31].

The modification involves the addition of a down-conversion (D-C) module to the basic design. This module reduces the feedback frequency to a value determined by the offset of the high-frequency source S1 from the OPLL output frequency. This frequency reduction offers the benefit of using low-frequency electrical components (power dividers, mixers, and amplifiers) after the D-C module, as well as providing continuous tunability of the microwave output [31].

The OPLL may also be configured to allow an information signal to be modulated onto one of the optical carriers. One such configuration is shown in Fig. 2. In this arrangement, the output from each laser diode (LD) is split into two branches, with one branch combining, as before, to form the feedback path, and the other branch recombining after one wavelength has been data-modulated to form the optical output signal.

One disadvantage of adding the high-frequency source for D-C is the introduction of additional phase noise into the system. Following a similar derivation as in [29], the additional phase noise contributed by the high-frequency reference source (S1) can be theoretically determined.

B. Phase Noise Analysis

In this analysis, it is assumed that the frequency discriminator does not contribute significantly to the phase noise at the output. This assumption is justified by the fact that the discriminator is designed to act only on the frequency error between the incoming signal and its set point and does not respond to the more quickly varying phase error [32]. Also, once the system is phase-locked, the frequency is highly stable; under this condition, the discriminator design indicates that its output is practically zero and therefore will not affect the beat signal.

Under these assumptions, referring to Fig. 1, the slave laser output can be written as

$$\frac{d\phi_s(t)}{dt} = K_{\rm o}K_{\rm d}\left[\sin\theta(t) + n'(t)\right] * f_{\rm fm}(t) * f(t) * f_{\rm pd}(t) * f_{\rm dc}(t) * f_{\rm amp}(t) * f_{\rm phot}(t) * \delta(t - T_d) \quad (1)$$

where $f_{\rm fm}(t)$, $f(t)$, $f_{\rm pd}(t)$, $f_{\rm dc}(t)$, and $f_{\rm phot}(t)$ represent the impulse responses of the slave laser FM response, loop filter, phase detector, D-C mixer, and PD, respectively, $f_{\rm amp}(t)$ incorporates the impulse responses of the amplifiers, and $\delta(t - T_d)$ represents the loop propagation delay. $K_{\rm o}$ is the slave laser gain factor, $K_{\rm d}$ is the phase detector conversion factor, and $n'(t)$ is the PD shot noise [21].

It is assumed that the master laser electric field $e_m(t)$, the slave laser electric field $e_s(t)$, the low-frequency source output voltage $v_r(t)$, and the high-frequency source output voltage $v_d(t)$ are given by, respectively

$$e_m(t) = E_m e^{j[\omega_m t + \phi_m(t)]} \quad (2a)$$

$$e_s(t) = E_s e^{j[\omega_s t + \phi_s(t)]} \quad (2b)$$

$$v_r(t) = A_r \cos\left[\omega_r t + \phi_r(t)\right] \quad (2c)$$

$$v_d(t) = A_d \cos\left[\omega_d t + \phi_d(t)\right] \quad (2d)$$

where E_m (volts per meter), E_s (volts per meter), A_r (volts), and A_d (volts) are the amplitudes; ω_m, ω_s, ω_r, and ω_d are the angular frequencies (radians per second); and $\phi_m(t)$, $\phi_s(t)$, $\phi_r(t)$, and $\phi_d(t)$ are the phases (radians) of the master

and slave lasers, and S2 and S1, respectively. The phase terms can be expressed as

$$\phi_m(t) = \phi_{\rm mo} + \gamma_m(t) \tag{3a}$$

$$\phi_s(t) = \phi_{\rm so} + \gamma_s(t) \tag{3b}$$

$$\phi_r(t) = \phi_{\rm ro} + \gamma_r(t) \tag{3c}$$

$$\phi_d(t) = \phi_{\rm do} + \gamma_d(t) \tag{3d}$$

where $\phi_{\rm mo}$, $\phi_{\rm so}$, $\phi_{\rm ro}$, and $\phi_{\rm do}$ are the quiescent phases and $\gamma_m(t)$, $\gamma_s(t)$, $\gamma_r(t)$, and $\gamma_d(t)$ are the phase fluctuations of the master laser, slave laser, S2, and S1, respectively.

In (1), $\theta(t) = \phi_{\rm ms}(t) - \phi_d(t) - \phi_r(t)$ is the phase error at the output of the phase detector, and $\phi_{\rm ms}(t) = \phi_m(t) - \phi_s(t)$.

Assuming that the phase error $\theta(t)$ in (1) is small enough to allow linearization of the system [i.e., $\sin\theta(t) \approx \theta(t)$], the closed-loop transfer function for the OPLL system is

$$H(s) = \frac{\phi_s(s)}{\theta(s) + \phi_s(s)} = \frac{KF(s)F_{\rm fm}(s)F_{\rm out}(s)e^{-sT_d}}{s + KF(s)F_{\rm fm}(s)F_{\rm out}(s)e^{-sT_d}} \tag{4}$$

where $F(s)$, $F_{\rm fm}(s)$, and $F_{\rm out}(s)$ are the Laplace transforms of the impulse responses of the loop filter, the slave laser FM response, and the combination of the other components, respectively, $K = K_{\rm o}K_{\rm d}$ is the total loop gain, and the noise term $n'(t)$ has been neglected.

The phase difference between the master and slave lasers, and the phase error at the output of the phase detector are, respectively

$$\phi_{\rm ms}(t) = \phi_{\rm mo} - \phi_{\rm so} + \gamma_m(t) - \gamma_s(t) \tag{5}$$

$$\theta(t) = \phi_{\rm mo} - \phi_{\rm so} - \phi_r(t) - \phi_d(t) + \gamma_m(t) - \gamma_s(t). \tag{6}$$

In (5) and (6), $\phi_{\rm so}$ is controlled by the loop to compensate for the phase fluctuations in the system. Therefore, by using the closed-loop transfer function $H(s)$, the Laplace transforms of $\phi_{\rm ms}(t)$ and $\theta(t)$ are

$$\begin{aligned}\phi_{\rm ms}(s) = {} & [1 - H(s)]\,[\Gamma_m(s) - \Gamma_s(s)] \\ & - H(s)\,[N'(s) - (\phi_d(s) + \phi_r(s))]\end{aligned} \tag{7}$$

$$\begin{aligned}\theta(s) = {} & [1 - H(s)]\,[\Gamma_m(s) - \Gamma_s(s) - (\phi_d(s) + \phi_r(s))] \\ & - H(s)N'(s)\end{aligned} \tag{8}$$

where $\Gamma_m(s)$, $\Gamma_s(s)$, and $N'(s)$ are the Laplace transforms of $\gamma_m(t)$, $\gamma_s(t)$, and $n'(t)$, respectively.

From (7) and (8), we see that the S1 phase term combines additively with the S2 phase. Therefore, the inclusion of the D-C module simply results in an increase in the phase noise level corresponding to the magnitude of S1's phase noise. If the high-frequency source is of high quality, with a lower phase noise level than S2, its impact on the overall system phase noise will be minimal.

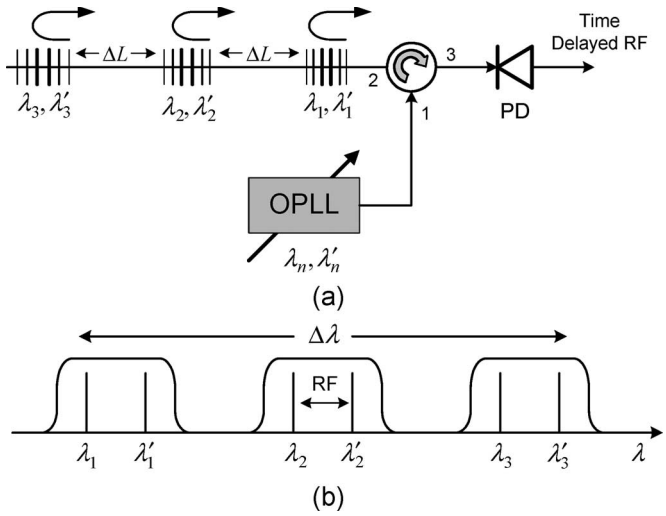

Fig. 3. (a) Schematic representation of a single delay line. (b) Theoretical spectral profile of a three-FBG delay line and the interaction of the RF-spaced wavelengths with each FBG. $\Delta\lambda$ is the overall spectral width of the delay line.

C. OPLL Wavelength Tuning

Wavelength tuning is accomplished in the OPLL setup through temperature control. Varying the thermoelectric cooler temperature causes a microscopic change in cavity length within each LD; thus, this property can be used to change the operating wavelength. The beat frequency depends only on the wavelength spacing; therefore, as long as both LDs are tuned by the same amount, the microwave output frequency is maintained. Temperature tuning of the wavelength is slow relative to current tuning, as it depends in part on the mechanical changes within the cavity. The speed of the wavelength change by temperature control was not measured with the understanding that a practical system would require the use of a quicker method, such as current tuning, to sweep the output wavelengths to provide agile beam steering.

D. FBG Delay Lines

The delay lines employed in this TTD system consist of three uniform FBGs. The central reflection wavelength of a uniform FBG is determined by the Bragg condition

$$\lambda_{\rm B} = 2n_{\rm eff}\Lambda \tag{9}$$

where Λ is the period of the FBG, $n_{\rm eff}$ is the effective refractive index of the fiber, and $\lambda_{\rm B}$ is the central reflection wavelength.

Fig. 3(a) and (b) shows the schematic representation and the theoretical reflection spectrum of a single delay line. In this system, the output wavelengths of the OPLL are temperature-tuned such that both λ_n and λ'_n are reflected within the same grating. The grating spectral width is an important characteristic since each grating must be able to reflect both wavelengths in order to avoid any corruption of the microwave output. Thus, the spectral width of each FBG imposes a limitation on the achievable microwave output frequency. In order to achieve a higher frequency, the FBG spectral width must be enlarged accordingly. In the case of a data-modulated signal, the data rate is, generally, much lower than the microwave signal

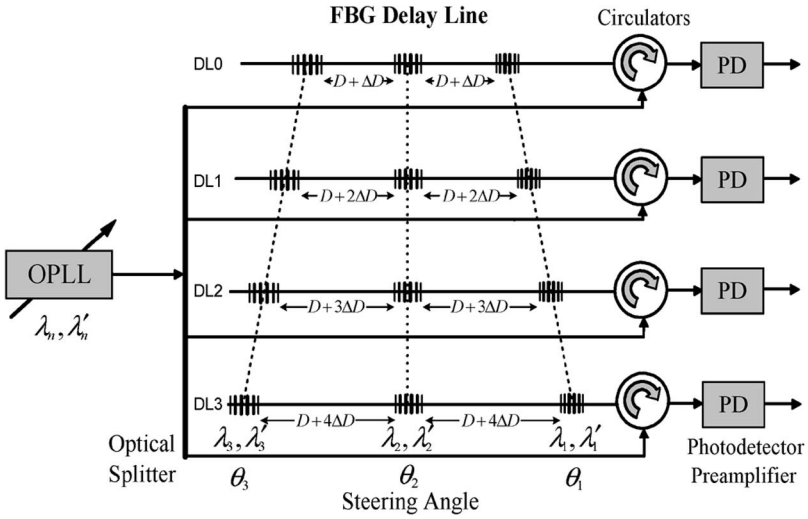

Fig. 4. TTD beamforming module consisting of four delay lines with three FBGs written on each delay line. OPLL: Optical phase-lock loop, PD: Photodetector.

frequency. Therefore, the optical sidebands are located very close to the OPLL wavelength that is modulated. Thus, the sidebands generated by DSB modulation would have a negligible impact on the FBG width required to reflect the signal.

By tuning the OPLL wavelengths to different values, the position of reflection along the delay line is changed. The recovered microwave signal after the PD has a particular phase corresponding to the time delay induced by the grating position. Precisely aligning the position of each FBG during the writing process controls the amount of phase shift induced by each delay line. In this arrangement, however, only discrete time delays are possible corresponding to the discrete positions of each individual FBG. Continuous tuning configurations are possible, for example, by the use of chirped, rather than uniform, FBGs.

The fact that the OPLL wavelengths are reflected from different positions within the same FBG can be a concern in maintaining the relative phase relationship between the two wavelengths. However, a uniform apodized grating can be properly designed such that it has a uniform group delay response across its passband [33] and, therefore, does not impart any additional relative delay to the two wavelengths.

Another important parameter for each FBG delay line is the overall spectral width $\Delta\lambda$. This width determines the wavelength tuning range that must be covered by the LDs of the OPLL. In this case, the OPLL setup uses two external cavity lasers (ECLs) which are not widely tunable. Therefore, achieving closely spaced FBGs, which do not interfere with each other and are within the ECL tuning range, is very important. A practical system would require many steering positions across a much broader wavelength range; thus, a widely tunable laser would be required.

E. TTD Beamforming Module

The TTD beamforming module is shown in Fig. 4. The key device in the module is the FBG prism, which is composed of four delay lines. Each delay line has three FBGs, which are fed by the OPLL via an optical power splitter and circulators. The FBGs along the same dashed lines are fabricated with identical central reflection wavelengths. By tuning the two optical wavelengths of the OPLL, λ_n, λ'_n, to a particular central reflection wavelength, different time delay progressions are generated, leading to different radiation directions [34]. The center gratings are all aligned such that they produce the same delay; thus, tuning the OPLL output to this wavelength will generate zero relative delay between the antenna elements and result in a broadside beam direction. Tuning the OPLL output to either the upper or lower wavelength grating produces a linear time delay progression and, hence, a linear phase progression, which will steer the antenna beam to a specific angle dependent on the magnitude of the phase progression.

The configuration shown in Fig. 4 is for the transmit mode of the antenna system. It may also operate in receive mode with slight modifications to the arrangement discussed in [34] or by the addition of a mixer at each antenna element, as suggested by Riza [23].

The physical parameter that determines the magnitude of the time delay progression is ΔD, the incremental distance between each FBG. This parameter determines the relative time delay of the signals arriving at the PAA elements and, therefore, the relative phase shift.

According to PAA theory, to avoid grating lobes (secondary maxima) in the beam pattern, the distance between each array element d must be

$$d \leq \frac{\lambda_{\mathrm{RF}}}{1 + |\sin\theta_{\max}|} \tag{10}$$

where λ_{RF} is the free-space wavelength of the microwave signal, and $\theta_{\max}$ is the maximum steering angle. It is assumed that $\theta_{\max} = \pm 90^{\circ}$; therefore, (10) becomes

$$d \leq \frac{\lambda_{\mathrm{RF}}}{2}. \tag{11}$$

For a frequency of 6.72 GHz, this maximum spacing is calculated as $d \leq 2.232$ cm. Simulation shows that a spacing of $d = 2.23$ cm produces minimal grating lobes and a well-defined mainlobe. For an N-element linear array, the incremental time

TABLE I
DELAY LINE SPACING

Delay Line Number	Delay Spacing, ΔL (mm)
DL 0	$D + 0$
DL 1	$D + 3.6$
DL 2	$D + 7.2$
DL 3	$D + 10.8$

delay required between each element to produce a steering angle θ of the mainlobe can be expressed as follows:

$$\Delta\tau = \frac{kd\sin\theta}{2\pi f_{\mathrm{RF}}} \tag{12}$$

where $k = 2\pi/\lambda_{\mathrm{RF}}$ is the free-space wavenumber, and θ is measured with respect to broadside.

For a $\pm 28^{\circ}$ steering angle, the time delay progression is calculated to be $\Delta\tau = 34.89$ ps. From this time delay value and n_{eff}, we can determine the incremental spacing required between each grating using

$$\Delta D = \frac{c\Delta\tau}{2n_{\mathrm{eff}}}. \tag{13}$$

This spacing is calculated to be $\Delta D = 3.6$ mm. The distance D in Fig. 4 is a constant spacing that exists between two adjacent FBGs. Theoretically, this constant spacing can be of any value as long as it is the same for each delay line. The important parameter is the difference in separation, which is governed by ΔD.

In all, four delay lines are fabricated with a linearly increasing separation ΔL between adjacent FBGs. The separation values are given in Table I.

III. RESULTS

This section presents the performance achieved by the OPLL and gives the spectral results for the FBG delay lines. It also gives an explanation of the experimental setup used and reports the measured time delays for the system.

A. OPLL

The OPLL uses two ECLs from K2 Optronics (ECCW Series) that have a listed linewidth of approximately 50 kHz [35]. This narrow linewidth eases the restriction that feedback time delay has on the loop operation [29], [36] and allows the use of off-the-shelf components for the feedback loop electronics [30]. Each ECL has a temperature tuning coefficient of approximately 16 pm/°C. This results in an overall wavelength tuning range of about 0.5 nm.

The two wavelengths are heterodyned on a new focus 45-GHz IR PD. Its output is amplified with an Agilent (83050A) broadband amplifier, and the output spectrum is measured with an Agilent 8565E Spectrum Analyzer. The output, a microwave carrier at 11.2 GHz, is shown in Fig. 5.

In order to make a comparison between the beat signal and the two microwave reference sources used in the system, the

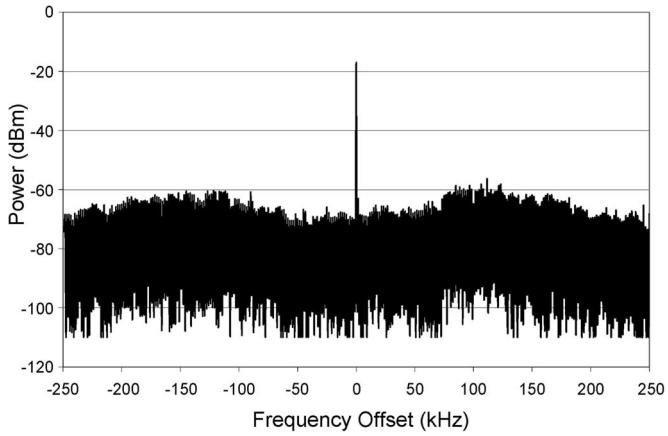

Fig. 5. Detected spectrum of the OPLL beat signal. Span = 500 kHz. Resolution bandwidth = 3 Hz.

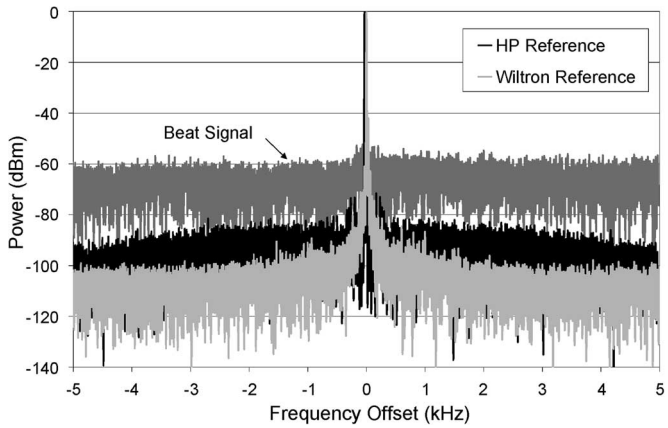

Fig. 6. Comparison of the OPLL beat signal with the two reference sources. Span = 10 kHz. Resolution bandwidth = 1 Hz.

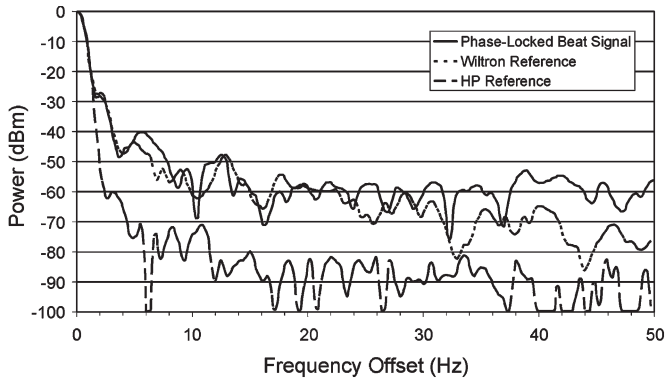

Fig. 7. Comparison of the OPLL beat signal with the two reference sources. Span = 50 Hz. Resolution bandwidth = 1 Hz.

spectra of all three are plotted on the same axes. The results are shown in Figs. 6 and 7, where the output power has been normalized to 0 dBm. The high-frequency reference S1 is a Wiltron 69387A source operating at 12 GHz, while the low-frequency reference S2 is an HP8648D source operating at 780 MHz. The quality of the phase-locked signal closely matches the quality of both reference sources near the carrier. The 3-dB bandwidths of all three signals are about 1 Hz.

The noise of the beat signal is slightly higher than either of the two reference sources. Further from the carrier, as shown in Fig. 6, the phase noise of the output signal is higher, around -60 dBm as compared to -90 and -100 dBm for the two reference sources. Practical beamforming applications would require a much lower phase noise level; therefore, the optimization of the system is required. However, this system performance is adequate to allow measurement of the time delays in the TTD system.

B. FBG Delay Lines

The FBGs used in this experiment are written based on the phase mask technique using a uniform 14-cm-long phase mask and an argon ion UV laser at 244 nm. Each delay line is written on a standard single mode fiber that has been hydrogen-loaded for approximately two weeks prior to exposure to increase its photosensitivity [37]. The fibers are stretched during the writing process to lower the reflection wavelength close to the operating wavelengths of the LDs [38], [39].

Stretching the fiber is necessary since only one suitably long phase mask is available. Its period of $\Lambda = 1072.2$ nm results in FBGs with a central wavelength near 1550.4 nm while the ECLs are operating near 1549 nm. Enough tension is applied to bring the FBGs below 1549 nm, and additional tension is added afterward to precisely align them with the ECL operating wavelengths. Along with the phase mask period and the writing wavelength, we can use the Bragg condition in (1) to determine the fiber's effective index. It is calculated to be $n_{\text{eff}} = 1.446$.

In order to obtain the time delay progression required for the TTD beamforming setup, it is important to precisely control the spacing of the three FBGs. Therefore, it is advantageous to write the three gratings on one fiber using a single uniform phase mask to cover the entire length of the delay line. In this case, a 14-cm-long phase mask is used which allows the three FBGs to be written without moving either the phase mask or the fiber during the writing process. The only adjustment necessary is a change in the applied tension to spectrally shift each central wavelength relative to the next.

Each FBG is 3-cm long and has a raised sine apodization profile [40]. Simulation shows that this profile gives good sidelobe suppression and allows the grating spectra to be spaced closely without interfering with each other. As stated in Section II-B, the close spacing is necessary since the tuning range of the ECLs is limited to only about 0.5 nm.

Typical transmission and reflection spectra of one of the delay lines are shown in Fig. 8. All three gratings have similar spectral profiles with 20–25-dB transmission depths and a spectral width of approximately 0.1 nm. Each FBG overlaps slightly with the adjacent one; however, the overlap is not significant within the transmission bandwidth. Therefore, the adjacent grating does not adversely affect the performance of its neighbor. In addition, the total spectral width covered by the three FBGs is well within the 0.5-nm tuning range of the ECLs.

As discussed in Section II-B, the spectral width is an important factor in the process since each grating has to be wide enough to reflect both wavelengths generated by the OPLL. In this case, the gratings are wide enough to accommodate a microwave spacing up to 12 GHz. This was easily wide enough to reflect the test signal wavelengths.

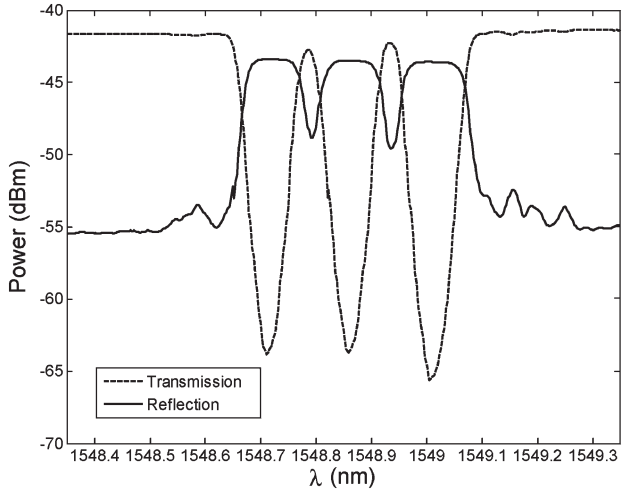

Fig. 8. Typical transmission and reflection spectra of a three-FBG delay line. The spectrum shown is for the $\Delta L = D + 10.8$-mm delay line.

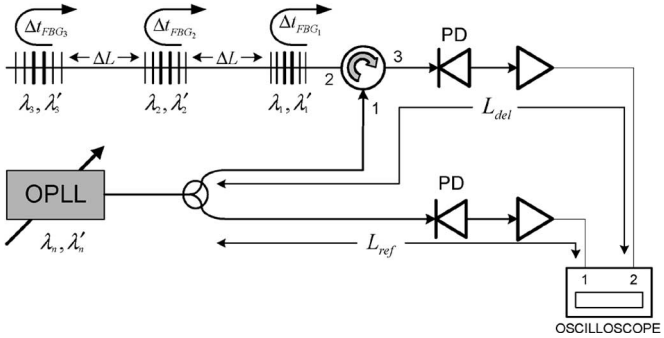

Fig. 9. Experimental setup used to measure relative time delays of each FBG delay line.

C. Time Delay Measurements

The goal of the measurement phase is to ensure that the OPLL will function with a TTD system and, then, to use this source to measure the time delays associated with each delay line to ensure that the correct phase shift can be recovered.

In the test setup, a single fiber delay line is clamped between a translation stage and a fixed stage, and tension is applied to adjust its reflection wavelength such that the center grating is aligned at 1549.2 nm. The OPLL is then engaged, and its operating point is tuned such that the two wavelengths are reflected by the center FBG of the delay line. The reflected signal is recovered by a PD and measured using an electrical spectrum analyzer (ESA). Fig. 9 shows the test setup used; however, in this first portion of the test, the recovered signals are individually input to the ESA, not the oscilloscope shown. This allows the quality of the signal reflected by the FBG to be analyzed. Fig. 10 shows the resultant signals, one from the reference (ref) path and the other from the delay (del) path.

By comparing these two signals, it can be seen that the reflected signal is very similar to the one recovered from the reference path. The 3-dB bandwidths are the same, and the noise

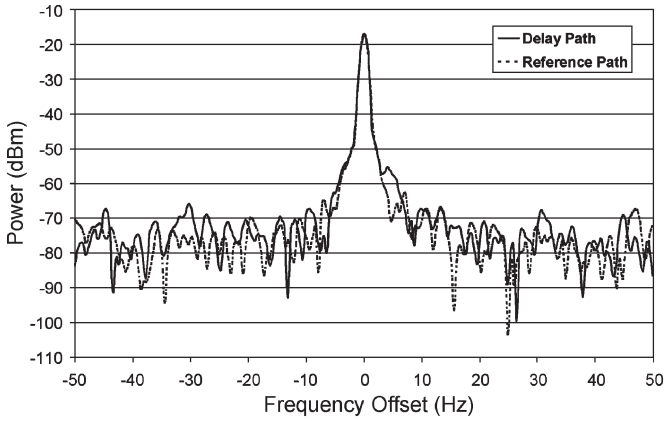

Fig. 10. Comparison of delay path and reference path signals.

levels are comparable. This confirms that an FBG can reflect the two wavelengths generated by the OPLL without losing the phase coherence established by the loop feedback.

The first time delay measurement test is done using the same setup shown in Fig. 9. It is carried out at 6.72 GHz since the maximum input frequency of the digital oscilloscope used in the measurement is 7 GHz. This frequency corresponds to a wavelength spacing of about 54 pm and is achieved by tuning S2 to an offset of 7.5 GHz and S1 to 780 MHz.

The measurement is based on a comparison between the reference path and the delay path phases. Comparing the reflected signal to the reference path for each FBG (three separate operating wavelengths) gives three phase values, which will be a function of the grating position and the path length traveled in the system. The relative phase, with respect to the center grating, of each upper and lower wavelength FBG can be determined by subtracting the individual phases from the center grating value. Since the setup uses an identical path for all three wavelength measurements, with the only difference being the reflection position, subtracting the phase values in this manner eliminates the effect of path length difference on the observed phase shift.

The electric field for each of the two LDs in the OPLL can be represented as

$$e_1(t) = E_1 \cos(\omega_1 t + \phi_{10}) \tag{14a}$$

$$e_2(t) = E_2 \cos(\omega_2 t + \phi_{20}) \tag{14b}$$

where E_1 and E_2 are the amplitudes (volts per meter), ω_1 and ω_2 are the angular frequencies (radians per second), and ϕ_{10} and ϕ_{20} are the initial phase angles of the electric fields (radian).

When these two fields are heterodyned on a square-law PD, the output is

$$\begin{aligned}|e_1(t) + e_2(t)|^2 = {} & \frac{1}{2}\left(|E_1|^2 + |E_2|^2\right) \\ & + \frac{1}{2}|E_1 E_2| \cos\left[(\omega_1 - \omega_2)t + \phi_{10} - \phi_{20}\right] \\ & + \frac{1}{2}|E_1 E_2| \cos\left[(\omega_1 + \omega_2)t + \phi_{10} + \phi_{20}\right].\end{aligned} \tag{15}$$

The first term on the right-hand side of the equation is a DC term, which has no effect on the output phase and can be neglected. The last term is the summed frequency term, which is well out of range of the PD bandwidth and can, therefore, also be neglected. The term of interest, then, is the difference frequency term that generates the microwave frequency output.

The OPLL is tuned to one of the three reflection wavelengths of the delay line, for example, λ_1, λ_1', and this optical signal is split at the optical power divider. Referring to Fig. 9, part of the optical signal is transmitted through the reference path to the oscilloscope input port. The measured voltage signal $v_{\rm ref}$ can be written as

$$v_{\rm ref} = \frac{1}{2} K_1 E_1 E_2 \cos(\omega_{\rm RF} t + \omega_{\rm RF} \Delta t_{\rm ref} + \phi_{10} - \phi_{20}) \tag{16}$$

where $\Delta t_{\rm ref}$ is the time taken to propagate along the reference path $L_{\rm ref}$, K_1 is a scaling factor incorporating the reference path PD conversion factor and the amplifier gain, and $\omega_{\rm RF}$ is the microwave frequency generated from the difference term $\omega_1 - \omega_2$.

The other part of the optical signal is transmitted along the delay path, which is reflected by $\rm FBG_1$ and input into the other oscilloscope port. The measured voltage signal $v_{\rm del}$ can be represented as

$$\begin{aligned}v_{\rm del} = {} & \frac{1}{2} K_2 E_1 E_2 \cos(\omega_{\rm RF} t + \omega_{\rm RF} \Delta t_{\rm del} \\ & + \omega_{\rm RF} \Delta t_{\rm FBG_1} + \phi_{10} - \phi_{20})\end{aligned} \tag{17}$$

where $\Delta t_{\rm del}$ is the time taken to propagate along the delay path $L_{\rm del}$, K_2 is a scaling factor incorporating the delay path PD conversion factor and the amplifier gain, and $\Delta t_{\rm FBG_1}$ is the round trip delay between the circulator and $\rm FBG_1$, as indicated in Fig. 9.

A phase difference comparison of the two input signals is done at the oscilloscope, giving

$$\phi_{\rm FBG_1} = \omega_{\rm RF}(\Delta t_{\rm FBG_1} + \Delta t_{\rm del} - \Delta t_{\rm ref}) \tag{18}$$

where the initial phase terms have canceled, and the remaining phase angle is a combination of the path length and the position of $\rm FBG_1$. Similarly, for $\rm FBG_2$ and $\rm FBG_3$, we can write

$$\phi_{\rm FBG_2} = \omega_{\rm RF}(\Delta t_{\rm FBG_2} + \Delta t_{\rm del} - \Delta t_{\rm ref}) \tag{19a}$$

$$\phi_{\rm FBG_3} = \omega_{\rm RF}(\Delta t_{\rm FBG_3} + \Delta t_{\rm del} - \Delta t_{\rm ref}). \tag{19b}$$

Now, using the center grating ($\rm FBG_2$) phase angle as the reference point and subtracting the other two phase angles from it, we obtain

$$\Delta\phi_{21} = \omega_{\rm RF}(\Delta t_{\rm FBG_2} - \Delta t_{\rm FBG_1}) \tag{20a}$$

$$\Delta\phi_{23} = \omega_{\rm RF}(\Delta t_{\rm FBG_2} - \Delta t_{\rm FBG_3}) \tag{20b}$$

where the contribution to the phase from the path length is now canceled. From these two phase values and the microwave frequency $\omega_{\rm RF}$, the time delays can be extracted.

$$\Delta t_{21} = \Delta t_{\rm FBG_2} - \Delta t_{\rm FBG_1} \tag{21a}$$

$$\Delta t_{23} = \Delta t_{\rm FBG_2} - \Delta t_{\rm FBG_3}. \tag{21b}$$

TABLE II
MEASURED TIME DELAYS

	Theoretical Time Delays	Experimental Time Delays at 6.72 and (6.03) GHz			Theoretical Time Delays
	Lower λ FBG (ps)	Lower Δt_{21} (ps)	Center Δt_{22} (ps)	Upper Δt_{23} (ps)	Upper λ FBG (ps)
DL0	0	0.58 (0.42)	0	-0.08 (-0.92)	0
DL1	+34.89	35.25 (35.83)	0	-34.92 (-37.50)	-34.89
DL2	+69.78	69.67 (72.17)	0	-70.50 (-70.25)	-69.78
DL3	+104.67	104.50 (106.92)	0	-105.17 (-102.92)	-104.67

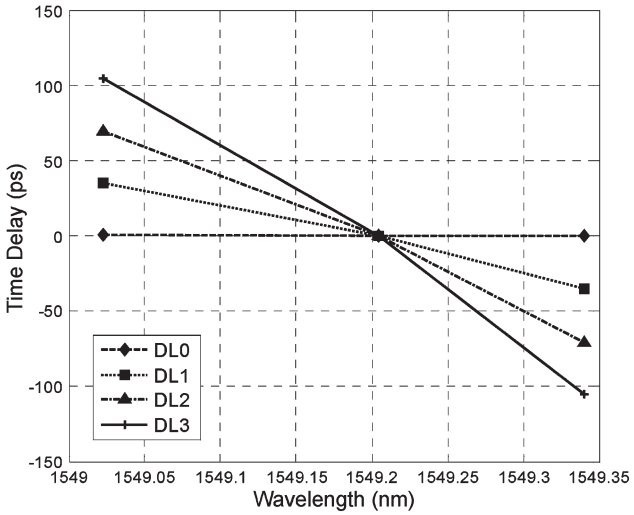

Fig. 11. Time delay progression of the measured delay values at 6.72 GHz.

These represent the amount of time for the round trip between adjacent FBGs on a single delay line.

All four delay lines are characterized at a microwave frequency of 6.72 GHz using this experimental method, which gives two sets of time delay values; one for the lower wavelength FBGs and one for the upper wavelength FBGs, all relative to the center grating of each delay line. These experimentally measured time delays are given in Table II, along with the theoretically calculated values. The measurement was then repeated at 6.03 GHz, a wavelength spacing of 46 pm, with the resultant values given in brackets in Table II. A measurement was done at this second frequency to verify the TTD nature of the system.

The delay contributed by the constant spacing D has been subtracted from the measurements reported in the table, and only the amount of additional delay from increments of ΔD is given.

It is evident from both measurements that a linear time delay progression is recovered, and this progression closely matches the designed time delay values calculated from (12). This result shows that an OPLL can be applied to a TTD beamforming system with successful recovery of the necessary time delays for beam steering.

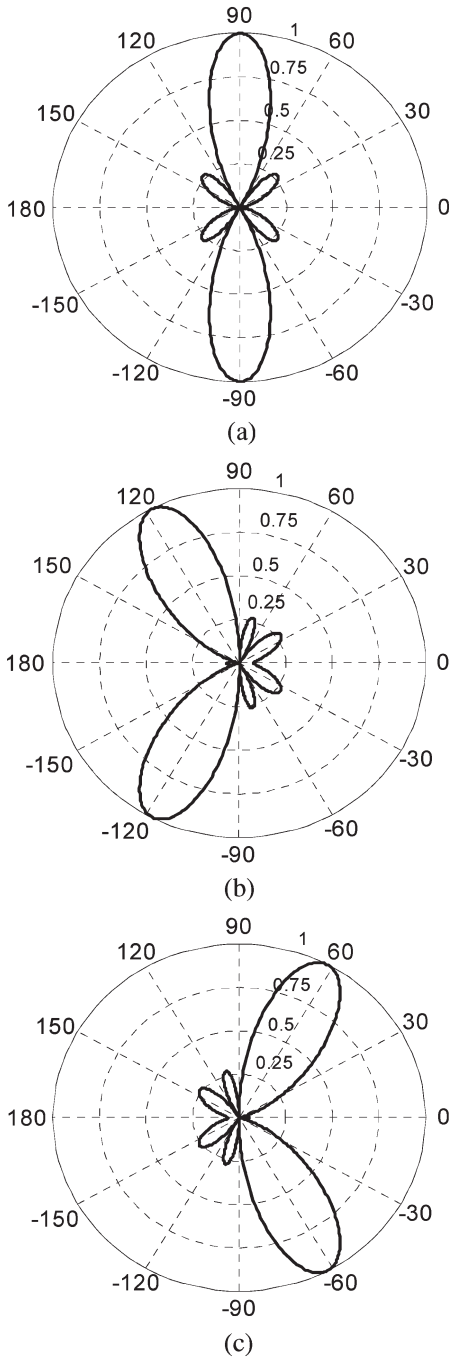

Fig. 12. Radiation patterns simulated from the experimentally measured time delay progressions at 6.72 GHz for (a) center wavelength delays → broadside beam, (b) lower wavelength delays → $+28°$ beam, and (c) upper wavelength delays → $-28°$ beam. Angles are shown with respect to antenna array axis.

The measured time delays for 6.72 GHz are plotted as a function of wavelength in Fig. 11. The even temporal spacing of each upper and lower grating away from the center FBG is represented by the linearity of the individual plot lines. The linear time delay progression is represented by the consistent step in slope apparent from one delay line plot to the next.

D. Simulated Antenna Radiation Patterns

Antenna radiation patterns can be simulated from the measured time delay data. These patterns are generated based on

a four-element linear array with an interelement spacing of 2.23 cm. The broadside pattern will be generated from the center gratings, which have zero relative delay. This output pattern is shown in Fig. 12(a). The lower and upper wavelength delay progressions generate the radiation patterns shown in Fig. 12(b) and (c), respectively. The delay progression is designed to give a steering angle of approximately $\pm 28^\circ$ from broadside. It can be seen that, when simulated, the experimentally measured time delays do, in fact, generate the designed steering angle.

IV. Conclusion

The application of a discriminator-aided OPLL to a uniform FBG TTD beamforming setup was realized and tested. Four discrete-FBG delay lines were designed and fabricated with a spectral width of about 0.1 nm near 1549 nm. The delay lines were designed such that the spacing between FBGs gave a time delay progression that would produce an approximately $\pm 28^\circ$ steering angle for a 6.72-GHz signal in a four-element PAA arrangement. The OPLL output signal quality was measured, and this signal was then applied to each delay line. The experimental time delays recovered closely corresponded to the designed values. The simulated radiation patterns generated closely matched the desired steering angle. To the best of our knowledge, this is the first application of an OPLL in a TTD beamforming setup. Further work is required to study other extensions of this application, including its use in continuous beamforming arrangements and the effect of superimposing data onto the generated RF carrier.

References

[1] R. A. Soref, "Fiber grating prism for true time delay beamsteering," *Fiber Integr. Opt.*, vol. 15, no. 4, pp. 325–333, Oct. 1996.

[2] A. Molony, C. Edge, and I. Bennion, "Fibre grating time delay element for phased array antennas," *Electron. Lett.*, vol. 31, no. 17, pp. 1485–1486, Aug. 1995.

[3] I. Frigyes and A. J. Seeds, "Optically generated true-time delay in phased-array antennas," *IEEE Trans. Microw. Theory Tech.*, vol. 43, no. 9, pp. 2378–2386, Sep. 1995.

[4] L. Xu, R. Taylor, and S. R. Forrest, "The use of optically coherent detection techniques for true-time delay phased array and systems," *J. Lightw. Technol.*, vol. 13, no. 8, pp. 1663–1678, Aug. 1995.

[5] R. A. Minasian and K. E. Alameh, "Optical-fiber grating-based beamforming network for microwave phased arrays," *IEEE Trans. Microw. Theory Tech.*, vol. 45, no. 8, pp. 1513–1517, Aug. 1997.

[6] A. Molony, L. Zhang, J. A. R. Williams, I. Bennion, C. Edge, and J. Fells, "Fiber Bragg-grating true time-delay systems: Discrete-grating array 3-b delay lines and chirped-grating 6-b delay lines," *IEEE Trans. Microw. Theory Tech.*, vol. 45, no. 8, pp. 1527–1530, Aug. 1997.

[7] Y. Chen and R. T. Chen, "A fully packaged true time delay module for a K-band phased array antenna system demonstration," *IEEE Photon. Technol. Lett.*, vol. 14, no. 8, pp. 1175–1177, Aug. 2002.

[8] D. N. McQuiddy, Jr., R. L. Gassner, P. Hull, J. S. Mason, and J. M. Bedinger, "Transmit/receive module technology for X-band active array radar," *Proc. IEEE*, vol. 79, no. 3, pp. 308–341, Mar. 1991.

[9] S. Blais, "Design and realization of a Bragg grating prism on planar integrated optical waveguides for wideband photonic true time-delay beamforming," Ph.D. dissertation, Dept. Elect. Eng., Univ. Ottawa, Ottawa, ON, Canada, 2005.

[10] R. C. Hansen, *Phased Array Antennas*. New York: Wiley-Interscience, 1998.

[11] P. Abele, R. Stephan, M. Birk, D. Behammer, H. Kibbel, A. Trasser, K. B. Schad, E. Sonmez, and H. Schumacher, "An electrically tunable true-time-delay line on Si for a broadband noise radar," in *Proc. Top. Meeting Silicon Monolithic Integr. Circuits RF Syst.*, Apr. 2003, pp. 130–133.

[12] N. A. Riza, *Photonic Control Systems for Phased Array Antennas* (SPIE Milestone Series), vol. 136. Bellingham, WA: SPIE, 1997.

[13] W. Ng, A. A. Walston, G. L. Tangonan, J. J. Lee, I. L. Newberg, and N. Bernstein, "The first demonstration of an optically steered microwave phased array antenna using true-time-delay," *J. Lightw. Technol.*, vol. 9, no. 9, pp. 1124–1131, Sep. 1991.

[14] R. D. Esman, M. Y. Frankel, J. L. Dexter, L. Goldberg, M. G. Parent, D. Stilwell, and D. G. Cooper, "Fiber-optic prism true time-delay antenna feed," *IEEE Photon. Technol. Lett.*, vol. 5, no. 11, pp. 1347–1349, Nov. 1993.

[15] G. A. Ball, W. H. Glenn, and W. W. Morey, "Programmable fiber optic delay line," *IEEE Photon. Technol. Lett.*, vol. 6, no. 6, pp. 741–743, Jun. 1994.

[16] D. T. K. Tong and M. C. Wu, "Programmable dispersion matrix using Bragg fiber grating for optically controlled phased array antennas," *Electron. Lett.*, vol. 32, no. 17, pp. 1532–1533, Aug. 1996.

[17] R. Benjamin and A. J. Seeds, "Optical beam forming techniques for phased array antennas," *Proc. Inst. Electr. Eng.—Pt. H*, vol. 139, no. 6, pp. 526–534, Dec. 1992.

[18] E. H. Monsay, K. C. Baldwin, and M. J. Caccuitto, "Photonic true time delay for high-frequency phased array systems," *IEEE Photon. Technol. Lett.*, vol. 6, no. 1, pp. 118–120, Jan. 1994.

[19] J. L. Corral, J. Marti, S. Regidor, J. M. Fuster, R. Laming, and M. J. Cole, "Continuously variable true time-delay optical feeder for phased-array antenna employing chirped fiber gratings," *IEEE Trans. Microw. Theory Tech.*, vol. 45, no. 8, pp. 1531–1536, Aug. 1997.

[20] J. L. Corral, J. Marti, J. M. Fuster, and R. I. Laming, "True time-delay scheme for feeding optically controlled phased-array antennas using chirped-fiber gratings," *IEEE Photon. Technol. Lett.*, vol. 9, no. 11, pp. 1529–1531, Nov. 1997.

[21] Y. Liu, J. Yang, and J. Yao, "Continuous true-time-delay beamforming for phased array antenna using a tunable chirped fiber grating delay line," *IEEE Photon. Technol. Lett.*, vol. 14, no. 8, pp. 1172–1174, Aug. 2002.

[22] M. Volker, "Coherent all-fibre optical beam-steering technique for phased-array antennas," *Proc. Inst. Electr. Eng.*, vol. 139, no. 4, pp. 305–308, Aug. 1992.

[23] N. A. Riza, "Acousto-optic liquid-crystal analog beam former for phased-array antennas," *Appl. Opt.*, vol. 33, no. 17, pp. 3712–3724, Jun. 10, 1994.

[24] R. Li and R. T. Chen, "3-bit substrate-guided-mode optical true time delay lines operating at 25 GHz," *IEEE Photon. Technol. Lett.*, vol. 9, no. 1, pp. 100–102, Jan. 1997.

[25] U. Gliese, T. N. Nielsen, S. Nørskov, and K. E. Stubkjaer, "Multifunctional fiber-optic microwave links based on remote heterodyne detection," *IEEE Trans. Microw. Theory Tech.*, vol. 46, no. 5, pp. 458–468, May 1998.

[26] R. Hofstetter, H. Schmuck, and R. Heidemann, "Dispersion effects in optical millimeter-wave systems using self-heterodyne method for transport and generation," *IEEE Trans. Microw. Theory Tech.*, vol. 43, no. 9, pp. 2263–2269, Sep. 1995.

[27] J. Park, W. V. Sorin, and K. Y. Lau, "Elimination of the fibre chromatic dispersion penalty on 1550 nm millimetre-wave optical transmission," *Electron. Lett.*, vol. 33, no. 6, pp. 512–513, Mar. 1997.

[28] G. H. Smith, D. Novak, and Z. Ahmed, "Overcoming chromatic-dispersion effects in fiber-wireless systems incorporating external modulators," *IEEE Trans. Microw. Theory Tech.*, vol. 45, pt. 2, no. 8, pp. 1410–1415, Aug. 1997.

[29] A. C. Bordonalli, C. Walton, and A. J. Seeds, "High-performance phase locking of wide linewidth semiconductor lasers by combined use of optical injection locking and optical phase-lock loop," *J. Lightw. Technol.*, vol. 17, no. 2, pp. 328–342, Feb. 1999.

[30] J. S. Seregelyi and J. C. Bélisle, "A discriminator-aided, optical phase-lock loop constructed from commercial components," in *Proc. SPIE, Photonics North*, 2004, vol. 5577, pp. 407–412.

[31] H. R. Rideout, J. S. Seregelyi, S. Paquet, and J. P. Yao, "Discriminator-aided optical phase-lock loop incorporating a frequency down-conversion module," *IEEE Photon. Technol. Lett.*, vol. 18, no. 22, pp. 2344–2346, Nov. 2006.

[32] A. Bononi, P. Ghiggino, and G. Picchi, "Analysis of the automatic frequency control in heterodyne optical receivers," *J. Lightw. Technol.*, vol. 10, no. 6, pp. 794–803, Jun. 1992.

[33] T. Erdogan, "Fiber grating spectra," *J. Lightw. Technol.*, vol. 15, no. 8, pp. 1277–1294, Aug. 1997.

[34] H. Zmuda, R. A. Soref, P. Payson, S. Johns, and E. N. Toughlian, "Photonic beamformer for phased array antennas using a fiber grating prism," *IEEE Photon. Technol. Lett.*, vol. 9, no. 2, pp. 241–243, Feb. 1997.

[35] R. E. Bartolo, C. K. Kirkendall, V. Kupershmidt, and S. Siala, "Achieving narrow linewidth, low phase noise external cavity semiconductor lasers through the reduction of 1/f noise," *Proc. SPIE*, vol. 6133, pp. 61 330I.1–61 330I.8, 2006.
[36] R. T. Ramos and A. J. Seeds, "Delay, linewidth, and bandwidth limitations in optical phase-locked loop design," *Electron. Lett.*, vol. 26, no. 6, pp. 389–391, Mar. 1990.
[37] A. Othonos, "Fiber Bragg gratings," *Rev. Sci. Instrum.*, vol. 68, no. 12, pp. 4309–4341, Dec. 1997.
[38] N. Sayers, S. Granieri, and A. Siahmakoun, "Fabrication of multiple fiber-Bragg gratings on one SMF using a single phase-mask," in *Proc. SPIE Photonic Appl. Devices and Commun. Syst.*, 2005, vol. 5970, p. 59 701J.
[39] Q. Zhang, D. A. Brown, L. Reinhart, T. F. Morse, J. Q. Wang, and G. Xiao, "Tuning Bragg wavelength by writing gratings on prestrained fibers," *IEEE Photon. Technol. Lett.*, vol. 6, no. 7, pp. 839–841, Jul. 1994.
[40] K. Ennser, M. N. Zervas, and R. I. Laming, "Optimization of apodized linearly chirped fiber gratings for optical communications," *IEEE J. Quantum Electron.*, vol. 34, no. 5, pp. 770–778, May 1998.
[41] Z. F. Fan and M. Dagenais, "Optical generation of a mHz-linewidth microwave signal using semiconductor lasers and a discriminator-aided phase-locked loop," *IEEE Trans. Microw. Theory Tech.*, vol. 45, no. 8, pp. 1296–1300, Aug. 1997.

Howard R. Rideout received the B.Eng. degree in electrical engineering from the Memorial University of Newfoundland, St. John's, NL, Canada, in 2004, and the M.A.Sc. degree in electrical engineering—microwave photonics, from the University of Ottawa, Ottawa, ON, Canada.

He is currently with the Communications Research Centre Canada (CRC), Ottawa. From 2005 to 2006, he worked in close collaboration with CRC on the development of an optical phase-lock loop system for radio-over fiber and software defined radio applications. His current research interests include microwave photonics, phased-array antennas, optical true-time delay techniques, and optical phase-lock loops.

Joe S. Seregelyi received the M.Eng. degree in engineering physics from McMaster University, Hamilton, ON, Canada, in 1987.

In 1988, he joined the National Research Council, where he was involved in the area of pulsed electromagnetics. Since 1993, he has been at the Communications Research Centre Canada, Ottawa, ON, where he is currently the Research Engineering/Project Leader of microwave photonics. He has authored or coauthored over 50 technical papers and reports. He is the holder of patents in the area of hybrid infrared (IR)/high-power microwaves (HPM) landmine detection and neutralization. He possesses extensive knowledge in the areas of RF and microwave design (signal integrity, circuit design, electromagnetic compatibility, antenna design, HPMs, and ultrawideband radar and communications). He has also been involved with optical design for a number of years (high-power lasers, antenna remoting, communications systems, and IR imaging).

Jianping Yao (M'99–SM'01) received the Ph.D. degree in electrical engineering from the Université de Toulon, Toulon, France, in 1997.

From 1999 to 2001, he held a faculty position with the School of Electrical and Electronic Engineering, Nanyang Technological University, Singapore. Since 2001, he has been with the School of Information Technology and Engineering, University of Ottawa, Ottawa, ON, Canada, where he is currently a Professor and Director of the Microwave Photonics Research Laboratory. He was a Guest Professor of Shantou University and Sichuan University, China, and was an Invited Professor with the Institut National Polytechnique de Grenoble, France, in 2005. His research has focused on microwave photonics, which includes all-optical microwave signal processing, photonic generation of microwave, millimeter-wave and terahertz, radio over fiber, ultrawideband over fiber, fiber Bragg gratings for microwave photonics applications, and the optically controlled phased-array antenna. His research interests also include fiber lasers, fiber-optic sensors, and biophotonics. He has published over 150 papers in refereed journals and conference proceedings.

Dr. Yao is a member of SPIE and OSA.